Evolutionary Gaps Stator Current Control of Multi-phase Drives Balancing Harmonic Content

Manuel R. Arahal, Federico Barrero, Manuel G. Satué, Cristina Martín and Mario Bermúdez

***Abstract*—Multi-phase machines are increasingly used in research and industry applications due to their inherent advantages. Stator current control is a common strategy for this type of systems. The most important issue it must face is regulation of currents in the torque producing plane and the harmonic plane. For this task, Finite Control Set Model Predictive Control (FCS-MPC) constitutes an interesting alternative to methods using modulation. However, the implementation of FCS-MPC is characterized by a high computational demand, limiting the sampling frequency. This work proposes a predictive algorithm that needs less computation time. As a result, the sampling period can be reduced while producing predictive control. This brings about several benefits resulting from improved current tracking. The proposed method avoids the combinatorial optimization phase of standard FCS-MPC which is the most time-consuming part. The algorithm is based on physical insights obtained from the application of FCS-MPC to multi-phase drives leading to the concept of evolutionary gaps regions. The experimental results for a five-phase motor demonstrate improved performance. Moreover, the method is flexible enough to balance the trade-off appearing between the torque producing plane and the harmonic plane.**

***Index Terms*—AC motor drives, Digital control, Multi-phase systems, Predictive control, Table lookup.**

I. Introduction

FINITE Control Set Model Predictive Control (FCS-MPC) has been proposed for electrical systems due to its flexibility to incorporate different objectives. This is particularly useful in multi-phase Induction Machines (IM), where several planes (not all torque producing) must be dealt with [1].

FCS-MPC is a direct digital control scheme where the control moves are the Voltage Source Inverter (VSI) configurations. Each configuration produces a voltage that is referred to as Voltage Vector (VV). The control action is obtained minimizing a cost function (CF) having several objectives balanced by Weighting Factors (WF). Previous works have considered parametric tuning of the CF [2]–[4], as well as the design of parameter-free CFs [5], [6]. However, it has been shown that trade-offs between figures of merit are unavoidable by simply adjusting the CF [7], [8]. Researchers have considered reducing the sampling period to improve current tracking. In addition, wide-band converters achieve high commutation frequencies, needing high sampling frequencies [9]. However, FCS-MPC is intensive in computation. As a result, a limit on the sampling frequency is found for any given computing hardware. Fast computation of the control action has become an interesting research topic in recent years. The case of three-phase converters is easier to study as there are no $x-y$ currents and the dynamics of the load is simpler [10]. The case of multi-phase drives is more demanding. One alley of research has been restraining the combinatorial space. For instance, in [11] the Voltage Vector (VV) search is restricted to an area within 60 degrees of the voltage space diagram. Similarly, in [12], an angular region is pre-selected to reduce the size of control set to 7 candidates for bipolar charging stations. Similarly, in [13], only the outermost maximum vector are considered for the optimization. However, these approaches do not fully utilize the VV set that the converter can produce. Avoiding this problem, in [14], a Sphere Decoding Optimization (SDO) algorithm is proposed to reduce the time needed to compute the control action. However, the reduction can be improved since SDO does not completely eliminate iterations.

Another research line is that of Virtual Voltage Vector also referred to as Synthetic Voltage Vector (SVV). The method aims at reducing the harmonic plane ($x-y$) content by issuing the VV in pairs [15]. The optimization is simplified as just the torque-producing plane is used. Also, the number of SVV is usually less than that of the full control set of VVs. For example, ten SVV are applied in [16] for a 5-phase VSI, 12 in [17] and 18 in [18]. Other proposals, related to SVV, use the deadbeat concept [19]. It must be also remarked that, in all SVV approaches $x-y$ currents are actually regulated in open loop, which is a major issue [20].

General methods for faster computation of the control action have also been used, for instance, Explicit Model Predictive Control (EMPC). EMPC is a technique where a quadratic programming problem is split into multiple local sub-problems each valid on a certain region [21]. Real-time implementation of the controller involves only the evaluation of the actual region to retrieve the appropriate control law. An example,

Manuscript received Month xx, 2xxx; revised Month xx, xxxx; accepted Month x, xxxx. This work was supported by Ministerio de Ciencia e Innovación of Spain, Agencia Estatal de Investigación, NextGenerationEU, grant TED2021-129558B-C22, and by Ministerio de Ciencia e Innovación of Spain, Agencia Estatal de Investigación, grant PID2021-125189OB-I00.

Manuel R. Arahal and Manuel G. Satué are with the Systems Engineering and Automation Department of the University of Seville, Seville, 41092, Spain (e-mail: arahal@us.es; mgarrido16@us.es).

Federico Barrero is with the Electronic Engineering Department of the University of Seville, Seville, 41092, Spain (e-mail: fbarrero@us.es).

Cristina Martín and Mario Bermúdez are with the Electrical Engineering Department of the University of Seville, Seville, 41092, Spain (e-mail: cmartin15@us.es; mbermudez4@us.es).

(Corresponding author Manuel G. Satué, phone: +34 954487353; fax: +34 954487353; e-mail: mgarrido16@us.es).

is [22], where the current control of a three-level neutral point clamped inverter is tackled. The current error and the voltage balancing of the capacitor are considered, dividing the space vector set into sectors. Although the method is viable, it has been reported that reducing the set of available VVs reduces flexibility. In [23] the EMPC technique is considered for a permanent magnet synchronous motor. Another EMPC algorithm is presented in [24], where pre-computed control laws represented by parameterized gains are provided. In both cases, instead of FCS-MPC a modulation block is used. Also, the region-dividing methodology is applied systematically, without realizing that a better partition is possible considering physical insights. In this regard, in [25] a new division that allows for faster computation is presented. However, the trade-off between $\alpha-\beta$ and $x-y$ planes is not tackled.

A. Novelty and Contributions

A fast method for the FCS-MPC optimization phase for stator current control of multi-phase IMs is presented. The justification for such proposal is the realization that a sampling period reduction benefits the drive operation [7]. The proposal explicitly considers the torque-producing plane ($\alpha-\beta$) and the harmonic plane ($x-y$). The method avoids the combinatorial optimization of FCS-MPC. As a result, the computational burden is lower than that of FCS-MPC. This allows for a reduction in sampling time which improves tracking. The proposal does not rely on SVV for the regulation of $x-y$ currents, instead they are considered in closed loop. Moreover, the proposed method is flexible enough to balance the trade-off appearing between $\alpha-\beta$ and $x-y$ planes.

The proposed method is related to EMPC but instead of providing control laws, it provides control actions. In this way, the method needs no modulation block. This allows for an increase in the control bandwidth compared to the case where modulation techniques (such as PWM) are used [26].

The novelty derives from the application of the Evolutionary Gap concept, which has been recently introduced by the authors. Such concept is based on insights obtained from the application of FCS-MPC to multi-phase IMs. It allows converting the combinatorial optimization into a region determination problem. Furthermore, the derivation of the regions is based on physical insights.

The rest of the paper is organized as follows. Section II presents the basics of FCS-MPC for controlling the stator current of a 5pIM. The proposed method is introduced in Section III, where an algorithm is given for its real-time implementation and is then evaluated using a laboratory setup in Section IV. The paper ends with a Conclusions section.

II. FCS-MPC for the Stator Current Control of 5pIM

In FCS-MPC, a predictive model provides predictions of stator currents for time $k+2$. The VSI state providing the lowest value for the CF is issued for the whole $k+1$ period. The predictive model is obtained discretizing the continuous-time IM equations as:

TABLE I
NOMENCLATURE

Electrical Variables	
i Current	v Voltage
ω Angular speed	T_L Torque load
Control Variables	
e Control error	E Root mean squared error
g Control Gap	H Rotor current term
N Number of points for root mean squared computation	
Q Quadrant	r Modulus of gap vector
ρ Active modulus	τ Active ratio
σ Auxiliary variable for look-up table access	
Control Parameters	
λ	Weighting factor of the CF
T_s	Sampling period
W_{xy}	Trade-off parameter
Drive Parameters	
L Inductance	R Resistance
P Pole pairs	V_{DC} Direct-Current voltage
Derived Coefficients	
$c_1 = L_s L_r - L_M^2$	$c_2 = L_r/c_1$
$c_3 = 1/L_{ls}$	$c_4 = L_M/c_1$
$a_2 = -R_s c_2$	$a_3 = -R_s c_3$
$a_4 = -L_M c_4 \omega_r$	$\gamma_h^c = \cos h\vartheta$
$\gamma_h^s = \sin h\vartheta$	$\vartheta = 2\pi/5$
δ Degradation	ξ Detuning factor
Subscripts and superscripts	
$\alpha-\beta$ Torque subspace	$x-y$ Harmonic subspace
c Correct	d Detuned
h Phase	i,j Matrix indices
$*$ Reference	$\hat{}$ Prediction

$$\hat{i}(k+1) = \Phi(\omega)i(k) + \Psi u(k) \tag{1}$$

where i contains stator currents on the α, β, x and y axes, $\hat{i}$ is the prediction, ω is the angular speed and u is the control signal, defined as $u = (K_1, K_2, \cdots, K_5)^\top$, where the values K_h indicate the state of the corresponding VSI switch for phases $h \in \{1,2,3,4,5\}$. Matrices Φ and Ψ are obtained from modeling and applying time discretization with sampling time T_s. This gives $\Phi = (I + AT_s)$, and $\Psi = T_s V_{DC} BTM$, where the following matrices are used.

$$A = \begin{pmatrix} a_2 & -a_4 & 0 & 0 \\ a_4 & a_2 & 0 & 0 \\ 0 & 0 & a_3 & 0 \\ 0 & 0 & 0 & a_3 \end{pmatrix}, B = \begin{pmatrix} c_2 & 0 & 0 & 0 \\ 0 & c_2 & 0 & 0 \\ 0 & 0 & c_3 & 0 \\ 0 & 0 & 0 & c_3 \end{pmatrix} \tag{2}$$

$$M = \frac{2}{5}\begin{pmatrix} 1 & \gamma_1^c & \gamma_2^c & \gamma_3^c & \gamma_4^c \\ 0 & \gamma_1^s & \gamma_2^s & \gamma_3^s & \gamma_4^s \\ 1 & \gamma_2^c & \gamma_4^c & \gamma_1^c & \gamma_3^c \\ 0 & \gamma_2^s & \gamma_4^s & \gamma_1^s & \gamma_3^s \\ 1/2 & 1/2 & 1/2 & 1/2 & 1/2 \end{pmatrix}, \tag{3}$$

The components of T are $T_{ii} = 4/5$ for the diagonal terms and $T_{ij} = -1/5$ for the off-diagonal terms. The DC link voltage (V_{DC}) and other coefficients are described in Table I. The two-step ahead predictions are found as

$$\hat{i}(k+2) = \Phi(\omega)\hat{i}(k+1) + \Psi u(k+1) + H(k) \tag{4}$$

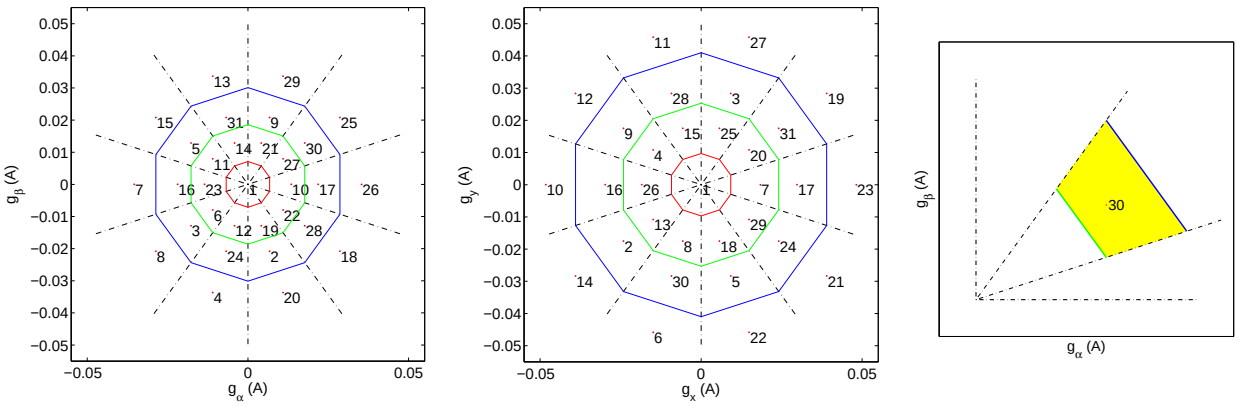

Fig. 1. Regions in gap space, projected to the $g_\alpha - g_\beta$ plane (left graph), to the $g_x - g_y$ plane (middle graph) and example of a region (right graph). The regions are identified by the index of the VV that is optimal for each one.

where H accounts for the effect of the rotor currents, which are usually unmeasured variables and can be estimated using a backtracking procedure (see [7]). The CF in imposes penalties on deviations of $\alpha-\beta$ and $x-y$ currents from their references using WF denoted as $\lambda_{\alpha\beta}$ and λ_{xy}. This results in

$$J(k+2) = \lambda_{\alpha\beta}\|\hat{e}_{\alpha\beta}(k+2)\|^2 + \lambda_{xy}\|\hat{e}_{xy}(k+2)\|^2 \quad (5)$$

where $\hat{e} \doteq i^* - \hat{i}$ denotes the predicted current error. During operation, the FCS-MPC tries to make the $\alpha-\beta$ components of stator currents follow a reference signal $i^*(k)$. The reference is a sinusoidal wave set by the speed/torque controller.

III. Proposal

The minimization of J in FCS-MPC is done by combinatorial search. This is a computationally expensive task, especially for multi-phase systems. The proposal in this paper is based on the distribution of optimal control actions with respect to a quantity termed gap that is defined in what follows.

According to equation (4), the prediction for $k+2$ is a function of the state predicted for $k+1$ and $u(k+1)$. Now, if one chooses to apply a null VV, then the evolution of stator currents is given solely by their own dynamics. The gap in $k+1$ is defined as the prediction of the control error for $k+2$ when a null VV is applied.

$$g(k+1) \doteq i^*(k+2) - A\hat{i}(k+1|k) + H(k) \quad (6)$$

where $g(k+1)$ is termed the evolutionary gap. If the control action applied does not correspond to a null VV, then Equation (4) allows one to write the predicted control error as

$$\hat{e}(k+2) = g(k+1) - \Psi u(k+1) \quad (7)$$

The theoretical justification of the proposal is based on the observation that the minimization of the CF given of (5) is related to the gap. Suppose that $\lambda_{\alpha\beta} \neq 0$ and $\lambda_{xy} = 0$, then the optimal VV depends just on $g_{\alpha-\beta}(k+1)$. Also the region in the subspace $g_{\alpha-\beta}$ where a particular VV is selected happens to be a convex region, more precisely a trapeze, as illustrated by Fig. 1. This is easily shown as the lines defining the trapezes are perpendicular bisectors of adjacent VVs. They are determined by equation (7) considering that the objective is achieving $\hat{e}(k+2) = 0$. Recall that the available control moves are the VV that the VSI can produce. Then, according to the previous definitions one gets $g(k+1) = T_s V_{DC} BTMu$, where u takes any of the 32 VSI states as is the common practice in FCS-MPC. This produces the 32 points shown on each plane in Fig. 1.

For the case where $\lambda_{\alpha\beta} = 0$ and $\lambda_{xy} \neq 0$ it is found that the optimal VV depends just on $g_{x-y}(k+1)$. Furthermore, the region in the subspace g_{x-y} where a particular VV is selected is again a trapeze. The more general case for $\lambda_{\alpha\beta} \neq 0$ and $\lambda_{xy} \neq 0$ can be treated by introducing a trade-off parameter W_{xy} to provide weighted values for the gaps. The subspace ($\alpha-\beta$ or $x-y$) that holds the largest weighted gap is used to define the actual table from which the control action is selected using the following algorithm.

In short, the proposal is supported by equations (6)-(7) and their connections with the control model of (4) and the cost function of (5). The available control moves can close the gap that might exist at any given sampling period. With this idea in mind, the concept is simple: closing the gap is equivalent to minimizing J.

A. Algorithm

According to the previous paragraphs, the control action can be decided by a table. The region where the gap is located must first be identified. This can be done following the steps of the flowchart of Fig. 2. In the flowchart (step 5), the computation of the quadrant of vector g^a is indicated as $\Gamma(g^a)$. Said vector is computed from $g(k+1)$ (steps 1 to 4) according to the relative values of $|(g_\alpha, g_\beta)|$ and $W_{xy}|(g_x, g_y)|$, where W_{xy} is a trade-off parameter. Parameters U_1 and U_2 are based on geometric considerations given the ten-fold symmetry of the regions, resulting in $U_1 = 1.3764$, $U_2 = 0.3249$. Parameters G_L, G_M, and G_S are based on the modulus of gaps. This set of parameters is machine dependent and can be computed from the equations of the model (1)-(4). They correspond to the midpoints between different VV coronas: Large (L), Medium (M) and Small (S). For example, G_L is the midpoint between L and M. For the case analyzed, the values for $\sigma = 1$ are

TABLE II
VV SELECTION TABLE

Cases		Quadrant $\sigma = 1$				Quadrant $\sigma = 0$			
σ_τ	σ_ρ	1	2	3	4	1	2	3	4
A	1	29	13	4	20	27	11	6	22
A	2	9	31	24	2	3	28	30	5
A	3	21	14	12	19	25	15	8	18
A	4	1	1	1	1	1	1	1	1
B	1	25	15	8	18	19	12	14	21
B	2	30	5	3	28	31	9	2	24
B	3	27	11	6	22	20	4	13	29
B	4	1	1	1	1	1	1	1	1
C	1	26	7	7	26	23	10	10	23
C	2	17	16	16	17	17	16	16	17
C	3	10	23	23	10	7	26	26	7
C	4	1	1	1	1	1	1	1	1

$G_S^{\alpha-\beta} = 0.0089$ (A), $G_M^{\alpha-\beta} = 0.0234$ (A), $G_L^{\alpha-\beta} = 0.0340$ (A). Similarly, for $\sigma = 0$ the values are $G_S^{x-y} = 0.0122$ (A), $G_M^{x-y} = 0.0318$ (A), and $G_L^{x-y} = 0.0515$ (A).

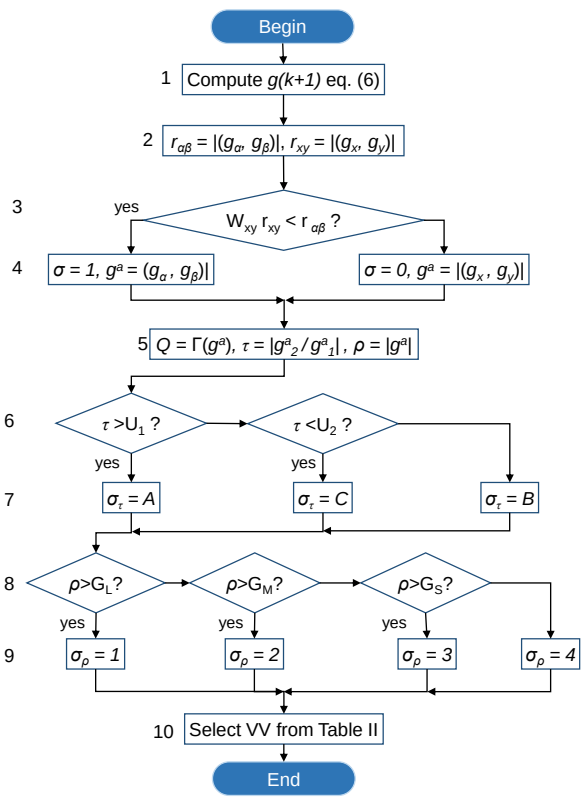

Fig. 2. Flowchart of the proposed algorithm.

B. Computational Cost

The reduction in computational effort attained by the proposal, in comparison with FCS-MPC, is due to the following.

- Step 1) involves matrix multiplication and 2 additions of 4-element vectors. Compared to FCS-MPC this operation has exactly the same complexity as one two-step ahead prediction computation using (4).
- Steps 2-4) need 2 2D-vector modulus operations for computing the r values, a scalar multiplication and a comparison to find the value of σ; then a 2D-vector assignation is needed to compute g^a.
- Step 5) requires two comparisons to find the quadrant Q, a division and scalar modulus to compute τ, and another 2D-vector modulus fo find ρ.
- Steps 6-7 need two comparisons to determine the case (A, B or C) and an assignation to determine σ_τ.
- Steps 8-9 require three comparisons to find σ_ρ.
- Step 10 needs a table search (based on σ, σ_τ, Q and σ_ρ) to obtain the VV index.

TABLE III
COMPARISON OF PROCESSOR TIMES (TMS320F28335).

Task	FCS-MPC	Proposal
A/D conversion	2.14 (μs)	2.14 (μs)
PI + delay compensation	1.80 (μs)	1.80 (μs)
Optimization	25.80 (μs)	**3.61** (μs)
Data logging and other processes	7.15 (μs)	7.15 (μs)

In contrast, the FCS-MPC algorithm needs 32 times the following: a 4×4 matrix multiplication and 2 additions of 4-element vectors (for the predictions), two vector modulus, a multiplication and an addition (for the computation of the CF). The processor times needed in both cases for a Texas Instruments digital signal processor (TMS320F28335) are presented in Table III. It can be seen that the proposal substantially reduces the requirements for the optimization phase.

IV. EXPERIMENTAL RESULTS AND COMPARISON

The experiments are carried out in a laboratory setup including: a 5pIM (with parameters given in Table IV), a VSI made by two SEMIKRON SKS 22F modules, a DC power supply, and a TMS320F28335 digital signal processor. Speed feedback is provided by a GHM510296R/2500 encoder. A DC motor is used to generate a torque load (T_L) for the different tests. The assessment of the controller is made using the current tracking error for N sample, as

$$E_{\alpha\beta} = \sqrt{\frac{1}{N}\sum_{k=1}^{N} e_{\alpha\beta}^2(k)}, \;\; E_{xy} = \sqrt{\frac{1}{N}\sum_{k=1}^{N} e_{xy}^2(k)}. \qquad (8)$$

A. Steady State Analysis

A series of tests have been performed to assess the proposal. Table V summarizes the results obtained comparing the performance of the proposed method with FCS-MPC (columns marked Std.) and with a method with less computational burden employing the technique of [13], where the number of VVs is restrained (columns marked Red). Columns marked G1 and G2 in Table V correspond to the proposed method

TABLE IV
PARAMETERS OF THE UTILIZED 5PIM

Parameter	Value	Unit
Stator resistance, R_s	12.85	Ω
Rotor resistance, R_r	4.80	Ω
Stator leakage inductance, L_{ls}	79.93	mH
Rotor leakage inductance, L_{lr}	79.93	mH
Mutual inductance, L_M	681.7	mH
Number of pairs of poles, P	3	-

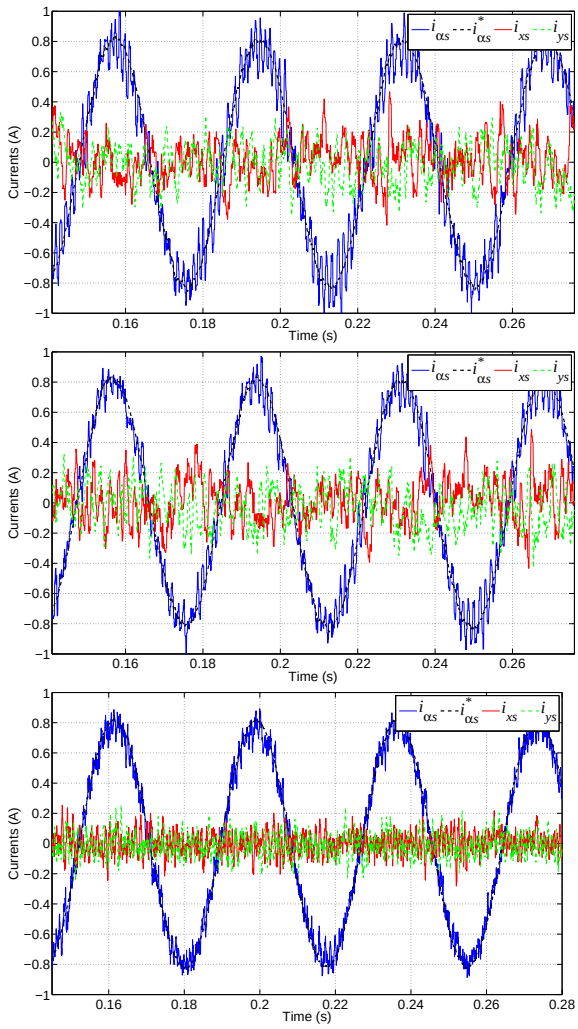

Fig. 3. Comparison of conventional FCS-MPC technique (top plot), a FCS-MPC with reduced computational burden (middle plot), and evolutionary gaps (bottom figure).

with $W_{xy} = 0.95$ and $W_{xy} = 0.5$ respectively. In said Table V, the tracking error is provided in (mA) to facilitate the reading. The sampling period for standard FCS-MPC is 50 (μs), 40 (μs) for FCS-MPC with reduced burden and 33 (μs) for the proposal.Three different operating points are considered, where different load torques are applied by an independent DC machine. For this, values of 10 %, 50 % and 100 % the nominal torque are used. The best result for each figure of merit is highlighted in bold for each test. The better

TABLE V
COMPARISON WITH STANDARD AND REDUCED BURDEN FCS-MPC

T_L	G1		G2		Std.		Red.	
(%)	$E_{\alpha\beta}$	E_{xy}	$E_{\alpha\beta}$	E_{xy}	$E_{\alpha\beta}$	E_{xy}	$E_{\alpha\beta}$	E_{xy}
10	99	**74**	**75**	74	113	108	99	112
50	135	**88**	**98**	88	142	109	125	114
99	190	**107**	**167**	133	221	113	181	115

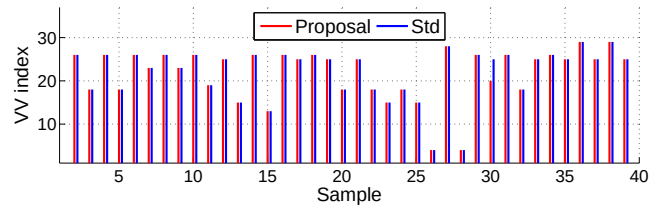

Fig. 4. Indices of voltage vectors selected by standard FCS-MPC and the proposal.

TABLE VI
RESULTS IN STEADY STATE FOR DIFFERENT VALUES OF W_{xy}

W_{xy}	$E_{\alpha\beta}$	E_{xy}	W_{xy}	$E_{\alpha\beta}$	E_{xy}
0.95	190	107	0.50	167	133
0.70	183	116	0.40	166	271
0.60	171	129	0.30	165	278

performance of the proposal is clearly visible.

In addition, Fig. 3 depicts stator currents for α and x axes. The top graphs correspond to Std FCS-MPC and the bottom ones to the proposal (G2 case). A reference speed $\omega_m^* = 500$ (rpm) is used. The sampling period for the FCS-MPC is 50 (μs) and 33 (μs) for the proposal. Current tracking is more accurate for the proposal, with less oscillations in α axis and less content in x axis.

A proof of the region's index of the VV in experimental results is provided by Fig. 4. The graph shows the VV selected by the standard FCS-MPC algorithm with combinatorial optimization (blue) and by the proposal (red). The agreement between the region based method and the combinatorial search method is remarkable. The small differences arise from the different way in which the trade-off between $\alpha - \beta$ vs. $x - y$ tracking is performed.

The harmonic distribution of the stator currents is shown in Fig. 5. The performance differences can be appreciated, where the proposed method shifts the harmonic content to higher frequencies while producing less Total Harmonic Distortion (THD).

The design parameter W_{xy} can be used to balance the trade-off between $\alpha - \beta$ tracking and $x - y$ regulation. Its effect on performance can be analyzed with the experimental hodographs of Fig. 6. On each graph, points laying on the outer corona are $(i_{s\alpha}, i_{s\beta})$ pairs. The corresponding $(i^*_{s\alpha}, i^*_{s\beta})$ values are presented with a dashed line. The points in the inner corona are (i_{sx}, i_{sy}) pairs. The left graph corresponds to a value $W_{xy} = 70$ and the right one to $W_{xy} = 35$. The

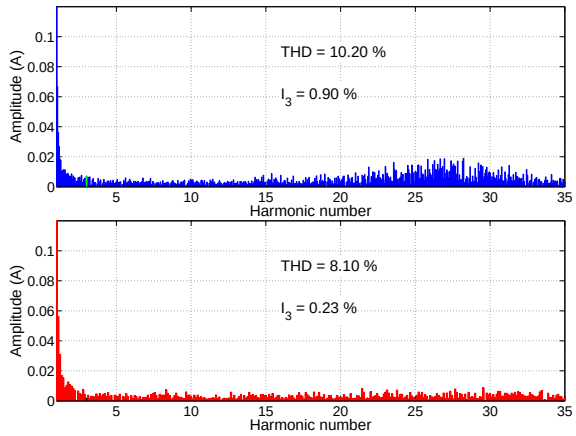

Fig. 5. Harmonic distribution for FCS-MPC (top) and the proposal (bottom). Values of THD and third harmonic amplitude (I_3) are provided.

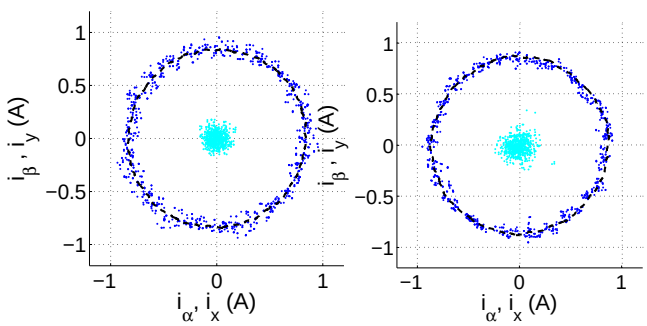

Fig. 6. Hodographs of stator currents in $\alpha - \beta$ plane (blue) and $x - y$ plane (cyan) for two values of the balancing parameter W_{xy}.

TABLE VII
EFFECT OF SAMPLING PERIOD

T_s (μs)	80	60	40	20
$E_{\alpha\beta}$ (mA)	162.54	122.70	82.32	41.61
E_{xy} (mA)	222.68	167.73	114.78	60.54

trade-off between $\alpha - \beta$ tracking versus $x - y$ regulation is clearly visible.

B. Effect of the Sampling Period

The effect of sampling period in the results can be checked with the help of Table VII, where the figures of merit are provided for several values usually found in the literature. It can be seen that a reduction in sampling time provides tighter control of $\alpha - \beta$ and $x - y$ stator currents. As an example consider the time trajectories of stator currents shown in Fig. 7. The sampling period for the proposal has been artificially increased to compare the results with standard FCS-MPC not having the computational burden reduction. In this case the proposal is run with $T_s = 40$ (μs) It can be seen that the better tracking of the proposal is hindered in this case, proving that the benefits of the method arise from the reduction in sampling period and not from the different treatment of the $\alpha - \beta$ and $x - y$ subspaces.

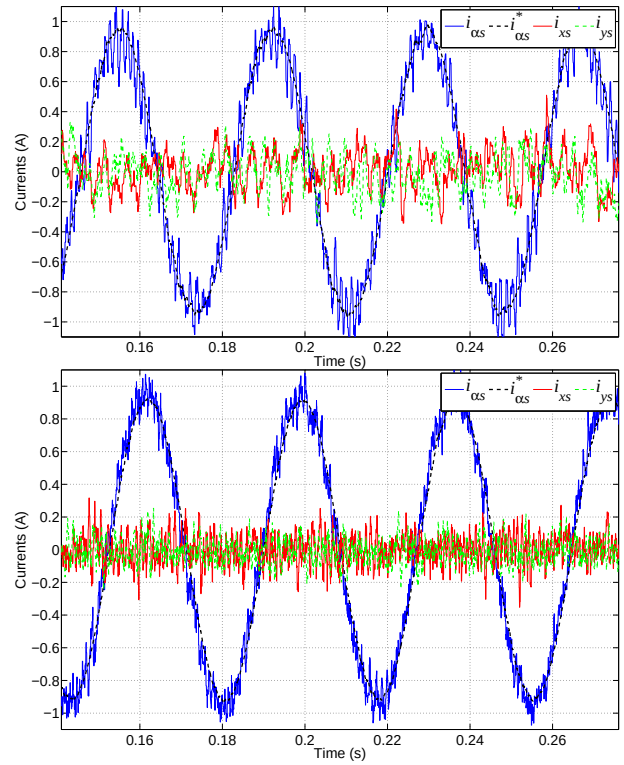

Fig. 7. Comparison of between FCS-MPC technique (top plot) and the proposal (bottom figure) for a different sampling period.

C. Transient Response Test

A reversal test is applied using a reference mechanical speed of ± 500 (rpm). During this test, the reference speed is abruptly changed from $+500$ (rpm) to -500 (rpm). The actual mechanical speed is monitored and included in the upper part of Fig. 8. In this way the proposed method is compared with a conventional FCS-MPC technique. Note that the outer speed control loops use the same PI tuning. The sampling period for the FCS-MPC is 50 (μs) and 33 (μs) for the proposal. In the lower part of said figures, the stator current reference i^*_{sq} computed by the PI is shown for both approaches. It can be seen that the proposed controller offers a speed regulation similar to that of the conventional FCS-MPC method, reducing the ripple of the torque-producing stator current, i_{sq}. In both cases the speed reversal is attained as expected.

D. Parametric Uncertainty Analysis

Parametric uncertainty is an important issue for model based controllers. For FCS-MPC, some papers have analyzed the effect of detuned models in performance [27], [28]. To avoid redundancies the present analysis is focused on those parameters that might have a more appreciable influence in the proposed method. In the following it is assumed that nominal parameters are those shown in Table IV, corresponding to the real system. The predictive model, however, will use other values computed as $\hat{R}_s = \xi_1 R_s$, $\hat{R}_r = \xi_2 R_r$, $\hat{L}_{ls} = \xi_3 L_{ls}$, $\hat{L}_{lr} = \xi_4 L_{lr}$. The different values of ξ_i provide the means to introduce various detuning situations. Please note that a value of $\xi = 0.5$ means that the model is using a parameter

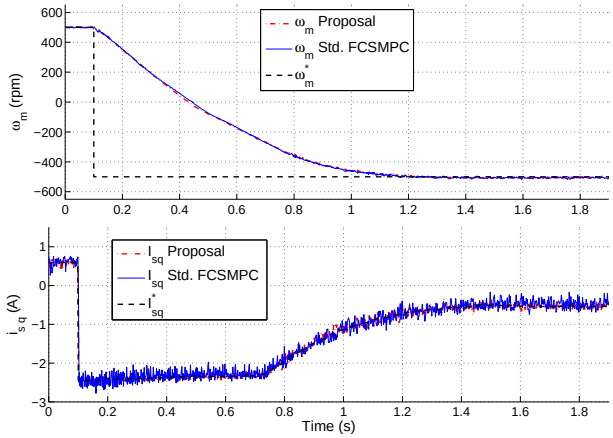

Fig. 8. Reversal test using the proposal (red) and FCS-MPC (blue).

TABLE VIII
EFFECT OF PARAMETRIC UNCERTAINTY.

Change	Conventional		Proposed	
	$\delta_{\alpha\beta}$	δ_{xy}	$\delta_{\alpha\beta}$	δ_{xy}
$\xi_1 = 0.5$	1.09	1.02	1.02	1.01
$\xi_1 = 2.0$	1.01	1.01	1.00	1.01
$\xi_2 = 0.5$	1.46	1.14	1.21	1.13
$\xi_2 = 2.0$	1.41	1.05	1.23	1.03
$\xi_3 = 0.5$	1.18	1.03	1.17	1.01
$\xi_3 = 2.0$	1.31	1.04	1.21	1.02
$\xi_4 = 0.5$	1.00	1.01	1.01	1.00
$\xi_4 = 2.0$	1.01	1.01	1.01	1.00

value half the correct value, $\xi = 1$ indicates no detuning and $\xi = 2$ implies that the model uses a parameter value double the correct one. In Table VIII the effect of the detuning is indicated as a degradation factor δ defined as $\delta = E^d/E^c$, where E is a figure of merit (either $E_{\alpha\beta}$ or E_{xy}). The superscript d indicates detuned parameter and the superscript c indicates correct value (i.e. $\xi_i = 1$ for all i). It can be seen that the uncertainty effect is less noticeable in the proposal due to the reduction in T_s.

Finally, Fig. 9 shows the results for a robust performance test. The stator current tracking can be compared with that of Fig. 3. Despite the use of a detuned model, the method is able to provide adequate control of stator current with little effect on performance.

E. Discussion and remarks

The reduction in sampling time provides results that are highlighted and analyzed in what follows:

- The proposal outperforms the conventional FCS-MPC technique in terms of the stator currents' indicators. This reduction in the figures of merit considered was anticipated in [7], and is a consequence of the reduction in the computational cost of the proposal. The experimental results show that the reduction in tracking error results from the reduction in sampling period and not from changes in the CF.
- The proposal is flexible in dealing with the trade-off between $\alpha - \beta$ tracking and $x - y$ regulation. This is clearly visible in the experimental results as the best values for the $\alpha - \beta$ tracking are always found for G2, while the best values for the regulation of the stator current components $x - y$ are found using G1.
- The proposal competes with standard FCS-MPC in terms of transient response. However, in this case, the outer PI tuning has a more appreciable effect. To ensure a fair comparison such tuning has been kept the same for both approaches.
- The problems associated with parameter uncertainty are less acute in the proposal. This is another positive effect of the reduction in sampling time. This is so because the model based controller receives a quicker feedback from the system.

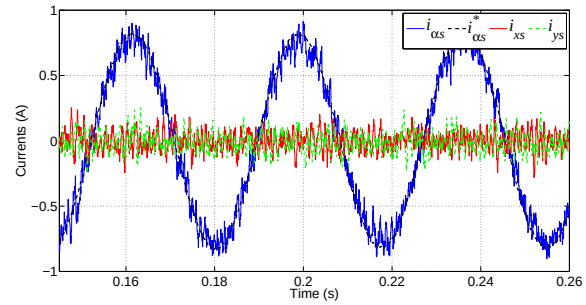

Fig. 9. Results for a robust performance test.

V. CONCLUSION

It has been shown that a faster computation of the control signal in FCS-MPC allows for a reduction in the sampling period. This in turn, produces better tracking of stator currents. As a result, other measures such as harmonic content are improved. As a side-effect, the proposal is better suited for its use with wide-band-gap semiconductor power devices.

A 5pIM has been used as a case example of the proposal. For higher number of phases the positive effects should be more noticeable as the combinatorial search of FCS-MPC would need more computations.

ACKNOWLEDGMENT

The research work has been funded by the Ministerio de Ciencia e Innovación of Spain, Agencia Estatal de Investigación, NextGenerationEU, grant TED2021-129558B-C22, and by the Ministerio de Ciencia e Innovación of Spain, Agencia Estatal de Investigación, grant PID2021-125189OB-I00.

REFERENCES

[1] A. Tenconi, S. Rubino, and R. Bojoi, "Model predictive control for multiphase motor drives–a technology status review," in *2018 International Power Electronics Conference (IPEC-Niigata 2018-ECCE Asia)*, pp. 732–739. IEEE, 2018.

[2] M. R. Arahal, C. Martín, A. Kowal, M. Castilla, and F. Barrero, "Cost function optimization for predictive control of a five-phase IM drive," *Optimal Control Applications and Methods*, vol. 41, no. 1, pp. 84–93, 2020.

[3] S. R. Mohapatra and V. Agarwal, "Model predictive controller with reduced complexity for grid-tied multilevel inverters," *IEEE Transactions on Industrial Electronics*, vol. 66, no. 11, pp. 8851–8855, 2018.

[4] X. Liu, L. Qiu, W. Wu, J. Ma, Y. Fang, Z. Peng, and D. Wang, "Neural predictor-based low switching frequency FCS-MPC for MMC with online weighting factors tuning," *IEEE Transactions on Power Electronics*, vol. 37, no. 4, pp. 4065–4079, 2021.

[5] K. Eshwar and V. K. Thippiripati, "Weighting-factorless predictive torque control scheme for dual inverter fed open-end-winding PMSM with single DC source," *IEEE Transactions on Power Electronics*, vol. 36, no. 11, pp. 12 968–12 978, 2021.

[6] V. Jayan and A. M. Ghias, "Weighting factor free model predictive control for a flying capacitor converter in a DC microgrid," *IEEE Transactions on Energy Conversion*, vol. 37, no. 2, pp. 1030–1041, 2021.

[7] M. R. Arahal, F. Barrero, M. J. Duran, M. G. Ortega, and C. Martin, "Trade-offs analysis in predictive current control of multi-phase induction machines," *Control Engineering Practice*, vol. 81, pp. 105–113, 2018.

[8] H. Fretes, J. Rodas, J. Doval-Gandoy, V. Gomez, N. Gomez, M. Novak, J. Rodriguez, and T. Dragičević, "Pareto optimal weighting factor design of predictive current controller of a six-phase induction machine based on particle swarm optimization algorithm," *IEEE Journal of Emerging and Selected Topics in Power Electronics*, 2021.

[9] A. González-Prieto, I. González-Prieto, M. Durán, and J. Aciego, "A memory-based model predictive control for multiphase electric drives using SiC switches," in *2022 International Conference on Electrical Machines (ICEM)*, pp. 136–142. IEEE, 2022.

[10] X. Liu, D. Wang, and Z. Peng, "A computationally efficient FCS-MPC method without weighting factors for NNPCs with optimal duty cycle control," *IEEE/ASME Transactions on Mechatronics*, vol. 23, no. 5, pp. 2503–2514, 2018.

[11] I. M. Alsofyani and L. M. Halabi, "Unidirectional finite control set-predictive torque control of ipmsm fed by three-level npc inverter with simplified voltage-vector lookup table," *Electronics*, vol. 12, no. 1, p. 252, 2023.

[12] H. T. Nguyen, K. Al Hosani, A. S. Al-Sumaiti, J. Y. Alsawalhi, K. A. Al Jaafari, T. H. Nguyen, and M. S. El Moursi, "Precise voltage regulation of unbalanced bipolar dc-grid based charging stations: A new multi-objective predictive control approach," *IEEE Transactions on Power Electronics*, 2023.

[13] H. Zhou, H. Li, X. Xiang, B. Yuan, T. Zhou, and W. Li, "Model predictive control algorithm of dual three-phase motor considering global single vector," in *2022 25th International Conference on Electrical Machines and Systems (ICEMS)*, pp. 1–6. IEEE, 2022.

[14] T. Dorfling, H. du Toit Mouton, T. Geyer, and P. Karamanakos, "Long-horizon finite-control-set model predictive control with nonrecursive sphere decoding on an FPGA," *IEEE Transactions on Power Electronics*, vol. 35, no. 7, pp. 7520–7531, 2019.

[15] M. G. Satue, M. R. Arahal, and D. R. Ramirez, "Estimation of rotor currents in polyphase machines for predictive control," *Revista Iberoamericana de Automática e Informática Industrial*, vol. 20, no. 1, pp. 25–31, 2023.

[16] B. Yu, W. Song, J. Li, B. Li, and M. S. Saeed, "Improved finite control set model predictive current control for five-phase VSIs," *IEEE Transactions on Power Electronics*, vol. 36, no. 6, pp. 7038–7048, 2020.

[17] S. Liu and C. Liu, "Virtual-vector-based robust predictive current control for dual three-phase PMSM," *IEEE Transactions on Industrial Electronics*, vol. 68, no. 3, pp. 2048–2058, 2020.

[18] P. Garcia-Entrambasaguas, I. Zoric, I. Gonzalez-Prieto, M. J. Duran, and E. Levi, "Direct torque and predictive control strategies in nine-phase electric drives using virtual voltage vectors," *IEEE Transactions on Power Electronics*, vol. 34, no. 12, pp. 12 106–12 119, 2019.

[19] M. S. Saeed, W. Song, B. Yu, and X. Wu, "Low-complexity deadbeat model predictive current control with duty ratio for five-phase PMSM drives," *IEEE Transactions on Power Electronics*, vol. 35, no. 11, pp. 12 085–12 099, 2020.

[20] C. Xue, W. Song, X. Wu, and X. Feng, "A constant switching frequency finite-control-set predictive current control scheme of a five-phase inverter with duty-ratio optimization," *IEEE Transactions on Power Electronics*, vol. 33, no. 4, pp. 3583–3594, 2017.

[21] A. Alessio and A. Bemporad, "A survey on explicit model predictive control," in *Nonlinear model predictive control*, pp. 345–369. Springer, 2009.

[22] M.-V. Doi, B.-X. Nguyen, and N.-V. Nguyen, "A finite set model predictive current control for three-level npc inverter with reducing switching state combination," in *2019 IEEE 4th International Future Energy Electronics Conference (IFEEC)*, pp. 1–9. IEEE, 2019.

[23] M. Zhao, Y. Cao, Y. Yan, Z. Zhang, T. Shi, and C. Xia, "Weighting factors tuning method in explicit model predictive direct speed control of permanent magnet synchronous motor," in *2021 24th International Conference on Electrical Machines and Systems (ICEMS)*, pp. 653–658. IEEE, 2021.

[24] K. Belda and P. Píša, "Explicit model predictive control of PMSM drives," in *2021 IEEE 30th International Symposium on Industrial Electronics (ISIE)*, pp. 01–06. IEEE, 2021.

[25] M. R. Arahal, F. Barrero, M. G. Satué, and M. Bermúdez, "Fast finite-state predictive current control of electric drives," *IEEE Access, 11, 12821-12828.*, 2023.

[26] C.-S. Lim, E. Levi, M. Jones, N. A. Rahim, and W.-P. Hew, "A comparative study of synchronous current control schemes based on FCS-MPC and PI-PWM for a two-motor three-phase drive," *IEEE Transactions on Industrial Electronics*, vol. 61, no. 8, pp. 3867–3878, 2013.

[27] C. Martin, M. Bermúdez, F. Barrero, M. R. Arahal, X. Kestelyn, and M. J. Durán, "Sensitivity of predictive controllers to parameter variation in five-phase induction motor drives," *Control Engineering Practice*, vol. 68, pp. 23–31, 2017.

[28] A. Altan and R. Hacıoğlu, "Model predictive control of three-axis gimbal system mounted on UAV for real-time target tracking under external disturbances," *Mechanical Systems and Signal Processing*, vol. 138, p. 106548, 2020.

Manuel R. Arahal was born in Dos Hermanas, Seville, Spain, in 1966. He received a master's degree and Ph.D. in Industrial Engineering from the University de Seville, in 1991 and 1996, respectively. He is currently a Full Professor with the Ingeniería de Sistemas y Automática Department, U. Seville. Prof. Arahal has received the Best Paper Awards from the IEEE Trans. on Ind. Electronics in 2009 and from the IET Electric Power Applications in 2010/2011.

Federico Barrero received the M.Sc. and Ph.D. degrees in electrical and electronic engineering from the University of Seville, in 1992 and 1998, respectively. In 1992, he joined the Electronic Engineering Department, University of Seville, where he is currently a Full Professor. Prof. Barrero was the recipient of the Best Paper Awards from the IEEE TRANSACTIONS ON INDUSTRIAL ELECTRONICS in 2009 and the IET Electric Power Applications in 2010/2011.

Manuel G. Satué was born in Seville, Spain. He received the master's degree in industrial engineering and the Ph.D. degree in industrial engineering from the University of Seville, Seville, Spain in 2008 and 2021, respectively.

His research interests include optimization for energy systems and predictive control. He is currently a Teaching Assistant with the with the Ingeniería de Sistemas y Automática Department, University of Seville.

Cristina Martín was born in Seville, Spain, in 1989. She received the Industrial Engineer degree from the University of Málaga, Spain, in 2014, and the Ph.D. degree in electrical/electronic engineering from the University of Seville, Spain, in 2020. She is currently a substitute professor in the Department of Electrical Engineering, University of Seville.

Mario Bermúdez was born in Málaga, Spain, in 1987. He received the B.Eng. degree in industrial engineering from the University of Málaga, Málaga, Spain, in 2014, and the Ph.D. degree in electrical/electronic engineering jointly from Arts et Métiers ParisTech, Lille, France, and from the University of Seville, Seville, Spain, in 2018. He is currently an Assistant Professor in the Department of Electrical Engineering, University of Seville.